5890 *Biochemistry* **2009,** *48,* 5890–5898
DOI: 10.1021/bi900305p

BIOCHEMISTRY
including biophysical chemistry & molecular biology
Article

Structure, Stability, and Folding of Ribonuclease H1 from the Moderately Thermophilic *Chlorobium tepidum*: Comparison with Thermophilic and Mesophilic Homologues[†]

Kathleen Ratcliff,[§,∥] Jacob Corn,[‡] and Susan Marqusee*[,‡,§,∥]

[‡]*Department of Molecular and Cell Biology, University of California, Berkeley, California 94720-3220,* [§]*Biophysics Graduate Group, University of California, Berkeley, California 94720, and* [∥]*Institute of Quantitative Biosciences (QB3)-Berkeley, University of California, Berkeley, California 94720*

Received March 2, 2009; Revised Manuscript Received April 8, 2009

ABSTRACT: Proteins from thermophilic organisms are able to function under conditions that render a typical mesophilic protein inactive. Pairwise comparisons of homologous mesophilic and thermophilic proteins can help to identify the energetic features of a protein's energy landscape that lead to such thermostability. Previous studies of bacterial ribonucleases H (RNases H) from the thermophile *Thermus thermophilus* and the mesophile *Escherichia coli* revealed that the thermostability arises in part from an unusually low change in heat capacity upon unfolding (ΔC_p) for the thermophilic protein [Hollien, J., and Marqusee, S. (1999) *Biochemistry 38*, 3831−3836]. Here, we have further examined how nearly identical proteins can adapt to different thermal constraints by adding a moderately thermophilic homologue to the previously characterized mesophilic and thermophilic pair. We identified a putative RNase H from *Chlorobium. tepidum* and demonstrated that it is an active RNase H and adopts the RNase H fold. The moderately thermophilic protein has a melting temperature (T_m) similar to that of the mesophilic homologue yet also has a surprisingly low ΔC_p, like the thermophilic homologue. This new RNase H folds through a pathway similar to that of the previously studied RNases H. These results suggest that lowering the ΔC_p may be a general strategy for achieving thermophilicity for some protein families and implicate the folding core as the major contributor to this effect. It should now be possible to design RNases H that display the desired thermophilic or mesophilic properties, as defined by their ΔC_p values, and therefore fine-tune the energy landscape in a predictable fashion.

Proteins from thermophilic organisms have the remarkable ability to remain folded and functional at temperatures where proteins from mesophiles are usually unfolded and inactive. Understanding the mechanisms by which these proteins have been optimized to function under such extreme conditions would provide great insight into the rules governing protein stability and thermodynamics. An obvious first step toward this goal is to compare the similarities and differences between sets of homologous proteins from thermophilic and mesophilic organisms. Such structural comparisons reveal that, as expected, the homologous proteins show nearly identical folds, and while specific changes in the side chains and their interactions can be seen, there are few generalizable rules (*1*−*7*). Similarly, sequence-based comparisons have been unable to determine any single model for thermal adaptation (*8*, *9*), concluding that residue-level control of energetics does not obey any obvious rules. Furthermore, the sequence similarity between thermophilic and mesophilic homologues is generally the same as that between two mesophilic homologues. Thus, there is no easy way to computationally determine whether a given protein originates from either a thermophilic or mesophilic organism.

Despite the difficulties in determining thermophilicity computationally, bioinformatic studies have found some general structural and sequence-based features that tend to correlate with the optimal growth temperature of organisms (*6*, *9*−*11*). None of these features are present in all thermophilic proteins, and there are exceptions to every rule that has been proposed. The simplest experimental approach employed to probe the basis of thermal stability in proteins has been to make point substitutions in mesophilic proteins that lead to an increased melting temperature (T_m) of the protein. The T_m of a specific protein can be naively increased by a simple residue replacement, resulting in introduction of specific stabilizing interactions. This approach, however, rarely results in a truly thermophilic protein but rather creates a hyperstable mesophilic protein (*12*, *13*).

Alternatively, thermodynamic characterization can usually differentiate between homologous thermophilic and mesophilic proteins. While the melting temperature of the thermophilic protein is generally higher than that of the mesophilic counterpart, studies on multiple pairs of thermophilic and mesophilic proteins show that they use various methods, including a change

[†]Research in S.M.'s laboratory is supported by Grant GM50945 from the National Institues of Health.

*To whom correspondence should be addressed. E-mail: marqusee@zebra.berkeley.edu. Telephone: (510) 642-7678. Fax: (510) 643-9290.

 Published on Web 05/01/2009

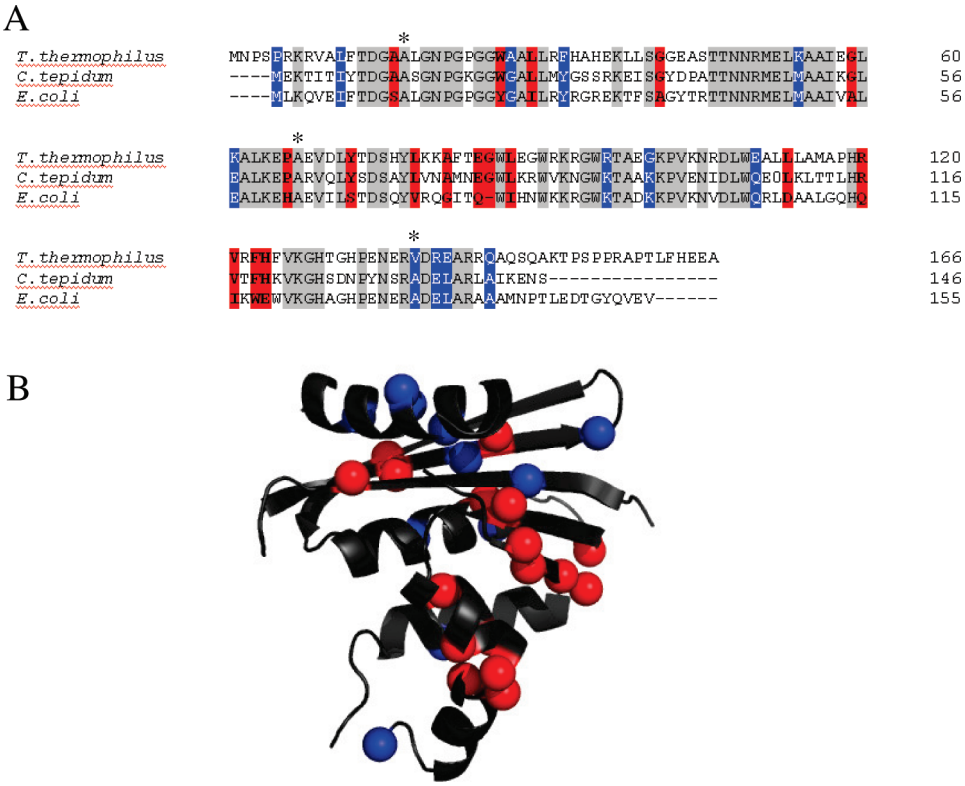

FIGURE 1: (A) Sequence alignment of *T. thermophilus*, *C. tepidum*, and *E. coli* RNases H* with conserved thermophilic residues colored red, conserved mesophilic residues blue, and invariant residues gray. Former cysteines in *C. tepidum* and *E. coli* RNases H are marked with asterisks above the residue in question. (B) Canonical RNase H fold (in this case, *C. tepidum* RNase H) with thermophilic residues shown as red spheres and mesophilic residues as blue spheres.

in enthalpy (ΔH), a change in heat capacity upon unfolding (ΔC_p),[1] or a change in overall stability (ΔG) (*14*−*18*), to tune their thermal stabilities.

Ribonuclease H (RNase H) has proven to be an excellent model protein for such thermodynamic studies. RNase H is a well-characterized nuclease that specifically digests the RNA strand of RNA−DNA hybrids. It is found in many different organisms, and in all cases examined, it folds into a single $\alpha+\beta$ domain ranging from 130 to 166 amino acids displaying the so-called RNase H fold (*1*, *19*). The energy landscapes of two RNases H, those from *Thermus thermophilus* and *Escherichia coli* (TthRNH and EcoRNH, respectively), have been extensively studied via thermal and chemical denaturation as well as hydrogen exchange (*16*, *20*, *21*). The stability curves (temperature vs ΔG_{unf} profile) show that, in addition to a higher melting temperature (T_m), TthRNH has a dramatically lower change in heat capacity upon unfolding (ΔC_p) and a higher overall stability (ΔG_{unf}) than EcoRNH (*19*). While the different ΔG_{unf} value was not unexpected, the variation in ΔC_p was quite surprising. Previous studies have determined that ΔC_p correlates strongly with the change in solvent-exposed surface area upon unfolding (ΔASA) (*22*), and because the two proteins bury a similar amount of nonpolar surface area when folded, it was expected that they would share similar ΔC_p values. After this was determined to not be the case, further studies revealed that the folding core of TthRNH is largely responsible for its low ΔC_p (*23*) and that substituting a single polar residue into the core region results in a more mesophile-like ΔC_p (*24*). Differential scanning calorimetry assigns the unusually low ΔC_p to an unexpectedly low absolute C_p of the unfolded state (*25*). All of these data can be explained by the hypothesis that TthRNH buries some hydrophobic surface area in the unfolded state (*23*, *25*). The residual structure is thought to arise from the core of TthRNH, but the nature of this residual structure and how it is encoded in the sequence is unknown. Experimentally, this has been particularly challenging, as the unfolded state is not significantly populated under native conditions. Moreover, whether this unusually low ΔC_p is a general feature of thermophilic proteins, or even thermophilic RNases H, is unclear.

To further probe the role of such residual structure in the unfolded state of thermophilic proteins, as well as to determine whether such behavior can be generalized to other thermophilic proteins, we have characterized a putative RNase H from the moderately thermophilic *Chlorobium tepidum*. *C. tepidum* has an optimal growth temperature (48 °C) between those of *E. coli* (37 °C) and *T. thermophilus* (68 °C) (*26*). These three RNases H have pairwise sequence identities greater than 50% and similarities greater than 70% (Figure 1). We have demonstrated that the putative protein is indeed an RNase H, determined the crystal structure of *C. tepidum* RNase H* (the asterisk denotes a cysteine-free variant of the protein), and determined that it shows few changes from the structures of the other two molecules, with an α-carbon root-mean-square deviation (rmsd) of <1.5 Å across all three proteins. We describe structural,

[1]Abbreviations: CD, circular dichroism; RNase H, ribonuclease H; ΔC_p, change in heat capacity upon unfolding; ΔG_{unf}, change in free energy upon unfolding ($G_u - G_f$); CtepRNH, ribonuclease H from *Chlorobium tepidum*; EcoRNH, ribonuclease H from *Escherichia coli*; TthRNH, ribonuclease H from *Thermus thermophilus*; CtepRNH*, cysteine-free version of ribonuclease H from *C. tepidum*; EcoRNH*, cysteine-free version of ribonuclease H from *E. coli*; TthRNH*, cysteine-free version of ribonuclease H from *T. thermophilus*; PDB, Protein Data Bank.

thermodynamic, and kinetic analyses of the moderately thermophilic RNase H homologue, which are suggestive of a low ΔC_p as a general property of thermophilic RNases H.

EXPERIMENTAL PROCEDURES

Cloning and Expression of C. tepidum RNase H. The ribonuclease H gene was amplified from *C. tepidum* genomic DNA (obtained from ATCC) by PCR using primers designed to add flanking KpnI and NdeI restriction sites, which were used to insert the gene into a pAED4 vector (*27*). Both strands of the coding region in the resulting plasmid (pKR203) were sequenced. Standard QuikChange (Stratagene) mutagenesis was used to create a cysteine-free variant in which all three cysteines were replaced with alanines (pKR201). The gene for wild-type CtepRNH was subcloned into a pET27 vector (Novagen) containing a thrombin site followed by an N-terminal six-His tag for ease of purification (pKR200). Plasmids encoding CtepRNH or CtepRNH* were transformed into *E. coli* BL21DE3 Codon+ cells (Novagen), and the cells were grown at 37 °C in Luria broth with 200 μg/mL ampicillin and 25 μg/mL chloramphenicol. Expression was induced at an OD_{600} of 0.6 by the addition of 1 mM IPTG, and cells were grown for an additional 3 h before being harvested by centrifugation.

Purification of C. tepidum RNases H. Purification of wild-type CtepRNH was conducted at pH 8.0 in the presence of fresh 1 mM tris(2-carboxyethyl)phosphine (TCEP). Cell pellets were resuspended in 50 mM Tris (pH 8.0), 20 mM NaCl, and 1 mM TCEP and lysed by sonication. The soluble fraction was loaded onto a HiTrap Heparin HP column from GE Healthcare and eluted with a linear NaCl gradient (from 0.02 to 0.8 M). Fractions containing RNase H were pooled, loaded onto a HisTrap nickel column from GE Healthcare {in nickel buffer A [20 mM $NaPO_4$ (pH 8.0), 0.5 M NaCl, 30 mM imidazole, and 1 mM TCEP]}, and eluted with a step to 500 mM imidazole. Pooled fractions were incubated overnight with thrombin to cleave the histidine tag and dialyzed back into nickel buffer A. His tag-free protein was reloaded onto the nickel column, the flow-through collected, and the resulting protein judged to be >98% pure by SDS−PAGE. CtepRNH* variants were purified similarly; however, in the sonication and heparin column purification steps, TCEP was omitted from all buffers and the nickel column was replaced with a Source 15S column. Fractions from the heparin column containing cysteine-free RNase H were pooled, loaded onto the Source 15S column [in 20 mM NaAc (pH 5.5), 200 mM NaCl, and 0.1 mM EDTA], and eluted with a linear NaCl gradient (from 0.2 to 0.6 M). Fractions were pooled and judged to be >98% pure by SDS−PAGE.

GdmCl-Induced and Thermal Denaturation. Circular dichroism (CD) measurements were taken on an Aviv 62DS spectropolarimeter with a Peltier temperature-controlled cell holder. For all samples described below, each CD measurement is an average of the signal at 222 nm for 1 min, in a 1 cm path length cuvette.

For experiments with CtepRNH, samples containing 50 μg/mL protein, 20 mM NaAc (pH 5.5), 50 mM KCl, 1 mM TCEP, and the appropriate concentration of GdmCl were allowed to equilibrate overnight before the CD signal was measured. For thermal denaturation, the CD signal was recorded every 3 °C, with a 5 min equilibration time and a 1 min averaging time at each temperature. At the end of the melt, reversibility was determined by returning to the beginning temperature and comparing the CD spectrum from 200 to 300 nm to the premelt spectrum. Experiments with the cysteine-free mutant *C. tepidum* RNase H* were conducted under identical conditions, but lacking TCEP.

GdmCl-induced denaturation of CtepRNH* was also performed by the serial addition of a solution containing protein at a high GdmCl concentration, 50 μg/mL protein, 20 mM NaAc, and 50 mM KCl (pH 5.5) to a starting solution containing the above without GdmCl. For each protein, the same starting and titrant solutions were used to measure the GdmCl-induced equilibrium unfolding at 10 different temperatures ranging from 5 to 50 °C. Additional data were collected by preparing 25 samples at varying concentrations of GdmCl and collecting temperature melts every 5 °C from 5 to 60 °C. Data from temperature melts at varying concentrations of GdmCl and data from GdmCl-induced melts at varying temperatures were both used for generation of the stability curves.

Denaturation and Stability Curve Data Analysis. Free energies of unfolding (ΔG_{unf}) were determined from GdmCl-induced denaturation of CtepRNH* at several temperatures, assuming a two-state model and a linear relationship between ΔG_{unf} and concentration of GdmCl (*28*). To determine the T_m for each protein, thermal melts were fit using a two-state model and the Gibbs−Helmholtz relationship between ΔG_{unf} and temperature (*29*). The resulting free energies of unfolding obtained from the denaturant melts were plotted as a function of temperature, with a single point added for the T_m ($\Delta G_{unf} = 0$). These data (ΔG_{unf} vs T) were fit to a modified Gibbs−Helmholtz equation (eq 1) using the T_m as a reference temperature:

$$\Delta G_{unf} = \Delta H^\circ - T\frac{\Delta H^\circ}{T_m} + \Delta C_p\left[T - T_m - T\ln\left(\frac{T}{T_m}\right)\right] \quad (1)$$

*Crystal Structure of CtepRNH**. CtepRNH* was crystallized by the hanging-drop method. Lyophilized protein was dissolved in water, resulting in a final protein concentration of 10 mg/mL. Crystals of CtepRNH*, were grown in 20% PEG 4000, 0.1 M Na HEPES (pH 7.5), and 10% 2-propanol, cryoprotected under the same conditions but with an additional 30% 2-propanol, flash-frozen in liquid nitrogen, and screened for diffraction. A full X-ray diffraction data set was collected at Stanford Synchrotron Radiation Laboratory beamline 11-1 from a crystal that diffracted to 1.6 Å.

To determine the crystal structure, more protein was expressed in minimal medium incorporating selenomethionine and again crystallized, this time from a final protein concentration of 5 mg/mL. The hanging-drop method was used to set new trays with SeMet CtepRNH*, resulting in crystals from a drop containing 26% PEG 4000, 0.2 M NH_3Ac, and 0.1 M NaAc (pH 5.4). Crystals were cryoprotected by addition of 30% MPD to crystallization conditions and flash-frozen in liquid nitrogen. Crystals were screened for diffraction and anomalous signal at LBNL ALS beamline 8.3.1. A SeMet crystal diffracted to 2.0 Å and was used for experimental phasing. The crystal structure from the native data set was determined, and models for each of the two molecules in the asymmetric unit were manually rebuilt using O (*30*). The model was further refined using the experimental phase restraints and RefMac (*31*). Data collection and refinement statistics are listed in Table 1. The structure has been deposited in the PDB as entry 3H08.

Solvent-accessible surface area calculations were performed using AREAIMOL for each molecule in the asymmetric unit cell of CtepRNH*, EcoRNH*, TthRNH*, and a chimera of EcoRNH* and TthRNH*, TCEO (PDB entries 1F21, 1RIL, and 1JL2, respectively) (*32*). Figures were made using PyMOL (*33*).

Refolding Kinetic Experiments. Folding kinetics of CtepRNH* were monitored at 25 °C by following the CD signal at 222 nm at various final urea concentrations (0.6−4.6 M). All folding data were collected on an Aviv 202 stopped-flow instrument. Folding was initiated by a 1:11 dilution of unfolded CtepRNH* [8 mg/mL protein, 6.3 M urea, 20 mM NaOAc, and 50 mM KCl (pH 5.5)] into folding conditions [20 mM NaOAc, 50 mM KCl (pH 5.5), and 0.6−4.6 M urea]. An average of seven kinetic traces (CD signal vs time) were collected for each condition *i*. The kinetic traces were fit to single-exponential equations ($A = Be^{-kt} + C$) using SigmaPlot (SPSS, Chicago, IL). The burst phase CD signal was determined by calculating the signal at time zero using the parameters determined by the fit (*B* and *C*). The final signal was determined by the fit parameter *C*. Both the burst phase and final signals at various urea concentrations were fit to obtain free energies of unfolding for the intermediate (ΔG_{ui}) and native (ΔG_{un}) states, respectively, assuming a two-state model and a linear dependence of ΔG on urea concentration (*28*).

Table 1: Data Collection and Refinement Statistics

	selenomethionine	native
space group	*P*1	*P*1
unit cell edges	33.74, 33.54, 66.49	33.46, 33.39, 66.07
unit cell angles	100.9, 99.1, 91.4	100.4, 99.4, 90.8
no. of molecules per asymmetric unit	2	2
	Data Collection Statistics	
wavelength (Å)	0.9794	1.1158
resolution[a] (Å)	50−2.10 (2.18−2.10)	50−1.60 (1.66−1.60)
no. of reflections (measured/unique)	236359/16590	85284/36214
R_{sym}[a] (%)	3.8 (9.2)	4.6 (9.3)
$\langle I/\sigma I\rangle$[a]	21.0 (8.8)	23.3 (8.3)
completeness[a] (%)	95.8 (95.7)	95.5 (92.8)
figure of merit (unflattened/flattened)		0.31/0.65
	Refinement Statistics	
resolution (Å)		50−1.6
R_{cryst}/R_{free} (%)		15.97/19.36
average *B*-factor (Å^2)		23.5
rmsd		
bond lengths (Å)		0.015
bond angles (deg)		1.32
no. of protein atoms		2399
no. of metal ions		2
no. of water molecules		299
Ramachandran (favored/allowed/generous/disallowed)		94.1/5.1/0.0/0.0

[a] Numbers in parentheses are for the highest-resolution shell.

RESULTS

Identification, Cloning, and Purification of a Putative RNase H from C. tepidum. A putative ribonuclease H gene from the bacterium *C. tepidum* was identified via a BLAST search (*7*) through homology to both *E. coli* and *T. thermophilus* RNases H. This gene was found to be 53% identical (65% similar) to EcoRNH and 57% identical (70% similar) to TthRNH. The gene was isolated from purified *C. tepidum* genomic DNA obtained from ATCC and subcloned into a pET27 vector. The resulting protein was overexpressed and purified via a two-column procedure (see Experimental Procedures). CtepRNH contains three cysteine residues at positions homologous to those of the three cysteines in *E. coli* RNase H. All three of these residues were mutated to alanine and subcloned into a pAED4 vector (*27*). The resulting protein, designated CtepRNH* [similar to the RNase H variants studied from *T. thermophilus* and *E. coli* (*16*, *34*)], was purified via heparin and ion exchange columns, as described in Experimental Procedures (*16*).

C. tepidum RNase H Folds into an Active Ribonuclease H*. Basic biophysical characterization revealed that both CtepRNH and CtepRNH* are folded and active. Circular dichroism (CD) spectra and denaturation profiles confirmed that both proteins have a high degree of secondary structure, suggesting a well-folded protein. The CD spectra are also consistent with the RNase H fold and similar to those found for other RNases H (*16*). RNase H activity assays (*23*, *35*) were performed, and the proteins were found to be active under standard assay conditions (Figure 2).

The Structure of C. tepidum RNase H Determined by X-ray Crystallography Reveals an RNase H Fold*. To confirm that CtepRNH* adopts the RNase H fold, the crystal structure was determined by single-wavelength anomalous

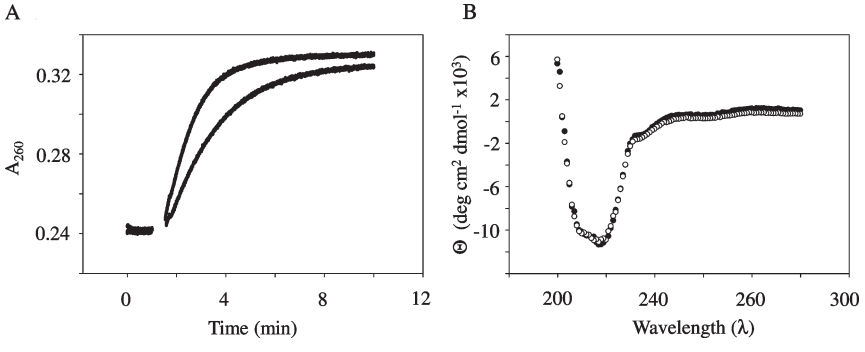

FIGURE 2: Biophysical attributes of *C. tepidum* RNase H*: (A) Activity assay of 20 and 50 nM *C. tepidum* RNase H* under standard assay conditions, as described in refs (*21*) and (*27*). (B) CD spectra of *C. tepidum* RNase H* taken before (●) and after (○) it had been heated to 90 °C. Data were taken on 50 μg/mL *C. tepidum* RNase H* at 25 °C in 50 mM KCl and 20 mM NaAc (pH 5.5).

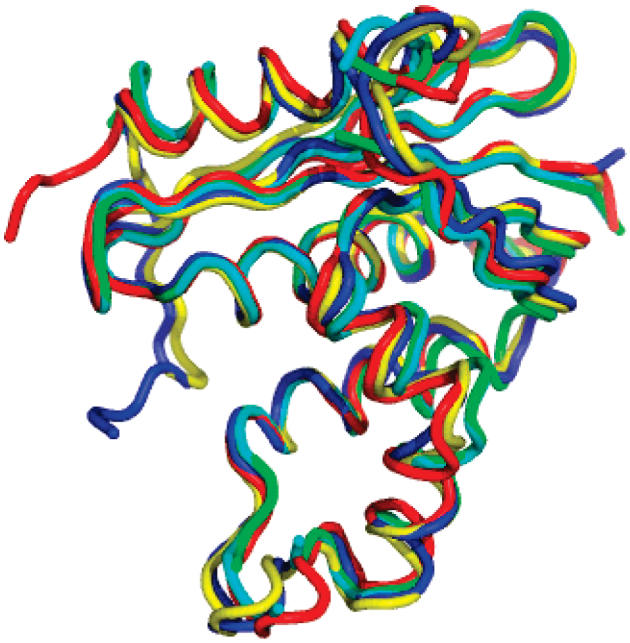

FIGURE 3: Superposition of the *E. coli* (blue), *C. tepidum* (green for chain A and aqua for chain B), TCEO (yellow), and *T. thermophilus* (red) RNases H*. The α-carbon backbones of all four proteins are aligned and have an rmsd of 1.45 Å.

dispersion (SAD) methods from selenomethionine-labeled protein to 1.6 Å resolution (see Experimental Procedures). The structure contains two molecules in the asymmetric unit, both of which adopt a fold identical to those of most other known RNase H structures. In fact, alignment of the α-carbons of CtepRNH* with those of EcoRNH*, TthRNH*, and a chimera of EcoRNH* and TthRNH* (TCEO) (*23*) yields pairwise rmsds of 1.288, 1.450, and 1.224 Å, respectively (Figure 3). In comparison, the two molecules in the CtepRNH* asymmetric unit (chain A and chain B) gave an rmsd of 0.440 Å. From our examination of the crystal structure, it is clear that there are no major structural differences between *C. tepidum* and the other RNases H*.

*Thermodynamic Characterization of C. tepidum RNase H**. The free energies of unfolding (ΔG_{unf}) of both wild-type and cysteine-free *C. tepidum* RNase H were determined by monitoring GdmCl-induced denaturation following both tryptophan fluorescence and the CD signal at 222 nm. The data were fit to a two-state model with a linear dependence of ΔG_{unf} on GdmCl concentration (*22*, *36*), resulting in a ΔG_{unf} at 25 °C of 8.1 ± 0.5 kcal/mol with an *m* value of 4.1 ± 0.5 kcal mol^{-1} M^{-1} for CtepRNH*. The results obtained via fluorescence and CD overlap well (Figure 4), indicating apparent two-state folding. The denaturant dependence, or *m* value, is similar to that obtained for other RNases H, as expected for homologous proteins (*22*). The ΔG_{unf} at 25 °C for CtepRNH is slightly higher (10.8 ± 0.9 kcal/mol). This stability difference between the wild-type and cysteine-free versions is comparable to the energetic difference between TthRNH and TthRNH* (13.3 and 12.2 kcal mol^{-1}, respectively). Thermal denaturation following the CD signal at 222 nm demonstrated reversible unfolding (Figure 2) with a T_m of 68.5 °C for wild-type and 66.5 °C for cysteine-free *C. tepidum* RNase H. Again, this difference is similar to that seen between *T. thermophilus* RNase H (89 °C) and its cysteine-free variant (86 °C) (*16*). In all of the following thermodynamic studies, the cysteine-free version

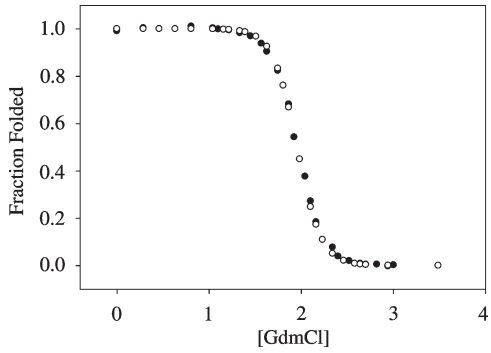

FIGURE 4: GdmCl-induced equilibrium denaturation monitored by CD (○) and tryptophan fluorescence (●). Data were taken for 50 μg/mL *C. tepidum* RNase H* at 25 °C in 50 mM KCl and 20 mM NaAc (pH 5.5) with varying concentrations of GdmCl.

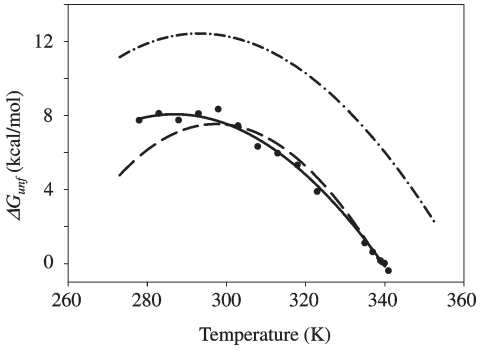

FIGURE 5: Protein stability curves of *E. coli* (– – –), *C. tepidum* (—●—), and *T. thermophilus* (– · –) RNases H*. Each point represents the average of two or three ΔG_{unf} values determined from isothermal GdmCl-induced denaturation experiments, with additional points for the T_m of *C. tepidum* RNase H*, determined by reversible thermal denaturation. Lines represent fits to the Gibbs–Helmholtz equation. Data were taken in 50 mM KCl and 20 mM NaAc (pH 5.5) with varying concentrations of GdmCl. *E. coli* and *T. thermophilus* RNase H* stability curves reproduced from ref (*16*).

was used and the results for it were compared to the results from previous studies using cysteine-free variants of *E. coli* and *T. thermophilus* RNase H (where wild-type cysteines were replaced with alanines in the case of EcoRNH or a combination of alanines and serines in the case of TthRNH*).

The ΔG_{unf} of CtepRNH* at various temperatures was determined to generate a protein stability curve, which plots stability as a function of temperature (*29*). To generate this profile, a minimum of three GdmCl-induced denaturant melts were obtained at each temperature, and the resulting ΔG_{unf} values for each melt were averaged. These averaged ΔG_{unf} values, along with a single point generated from the thermal denaturation data for the T_m ($\Delta G_{unf} = 0$), were fit to the Gibbs–Helmholtz equation (eq 1) (*29*, *36*). The resulting curve and the individual stability measurements are plotted in Figure 5, along with the results from the previous studies on *E. coli* and *T. thermophilus* RNases H*. CtepRNH* clearly has a broader stability curve than EcoRNH* as reflected in a smaller change in heat capacity upon unfolding (Table 2). Surprisingly, the value obtained for the ΔC_p of CtepRNH* is very similar to that of TthRNH* while most other thermodynamic parameters are closer to those of EcoRNH* (Table 2).

Table 2: Thermodynamic Parameters of *E. coli*, *C. tepidum*, *T. thermophilus*, and a quintuple mutant of *E. coli* RNases H*[a]

	ΔG_{unf} (kcal/mol)	ΔG_{growth} (kcal/mol)	T_{growth} (°C)	ΔC_p (kcal mol^{-1} K^{-1})	T_m (°C)
E. coli RNase H*	−7.5	−6.8	37	2.7	67
C. tepidum RNase H*	−8.1	−4.6	48	1.7	66.5
T. thermophilus RNase H*	−12.2	−5.6	68	1.8	86
E. coli 5H-RNase H	−11.9	−11.0	37	2.7	79

[a] Data for *E. coli* and *T. thermophilus* RNases H* taken from ref (*16*). Data for *E. coli* 5H-RNase H taken from ref (*13*). *E. coli* 5H-RNase H also contains all three natural cysteines.

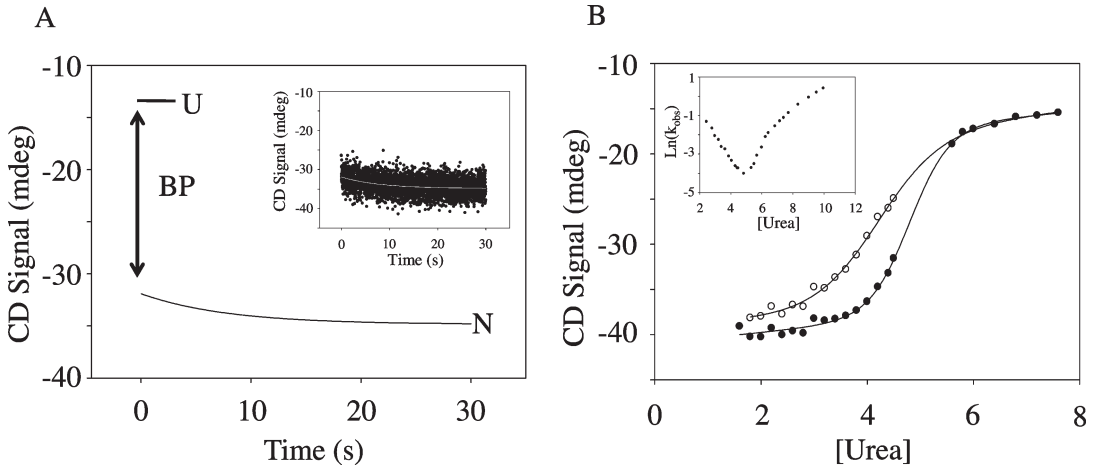

FIGURE 6: Kinetics of *C. tepidum* RNase H*. (A) Refolding of *C. tepidum* RNase H* in 2.8 M urea. Refolding was initiated by rapid dilution of unfolded protein (6.3 M urea) into folding conditions [20 mM NaOAc and 50 mM KCl (pH 5.5) with various urea concentrations] and was monitored by circular dichroism (inset). Solid lines are fits of the data to single-exponential equations. U represents the signal of the unfolded state, N the signal of the folded state, and BP the magnitude of the burst phase signal. (B) Burst phase (○) and final (●) amplitudes from kinetic experiments at 20 mM NaOAc and 50 mM KCl (pH 5.5) and various urea concentrations. The inset shows the observed rates for each concentration of urea taken, a "chevron" plot.

*Probing the Folding Pathway of C. tepidum RNase H**. To evaluate the energy landscape of CtepRNH* and determine if, like the well-characterized EcoRNH* and TthRNH*, the protein has a fast folding core, we evaluated its folding kinetics using stopped-flow circular dichroism. The time course of folding and unfolding was followed by monitoring the CD signal at 222 nm at various final urea concentrations. As has been seen with all other RNases H studied in this manner, at low concentrations of denaturant (< 3 M urea), CtepRNH* has a large burst phase upon refolding, with > 75% of the CD signal lost in the dead time of the instrument (12 ms), followed by the remaining folding process, which occurs on a slower, measurable, time scale (Figure 6A). Below ~2 M urea, the amplitude of this burst phase dominated the signal change to the extent that we could no longer confidently fit the remaining data (< 10% signal change in the observable phase).

These data suggest that, like EcoRNH* and TthRNH*, CtepRNH* folds in a three-state manner, populating a refolding intermediate at low concentrations of denaturant. The folding process was modeled as a three-state, on-pathway process, in which the intermediate is an obligatory step in the folding process. Indeed, single-molecule refolding data from EcoRNH* have shown that the intermediate of RNase H is on-pathway (*37*). The amplitude of the burst phase signal was fit independently (U and I) to determine the free energy of unfolding for the intermediate, ΔG_{ui}, and its linear dependence on urea, m_{ui}. On the basis of this analysis, we determined the stability of the intermediate of CtepRNH* to be 4.1 ± 1 kcal/mol, with an m_{ui} value of 1.0 ± 0.1 kcal mol^{-1} M^{-1}. The stability of the intermediate falls directly between those of the intermediates of EcoRNH* and TthRNH* (3.5 and 4.5 kcal/mol, respectively), with similar m values (1.2 and 1.0 kcal mol^{-1} M^{-1}). Data points taken from the final amplitude change observed in these kinetic studies were also fit to a two-state model (U and N), and the resulting ΔG_{unf} is 7.5 ± 0.9 kcal/mol with an m value of 1.6 ± 0.2 kcal mol^{-1} M^{-1} (Figure 6B). As expected from other studies on RNases H, the ΔG_{unf} determined from urea is slightly lower than that determined by GdmCl-induced denaturation studies (7.5 ± 0.9 kcal/mol vs 8.1 ± 0.5 kcal/mol).

The rates for each final concentration of denaturant were fit and plotted to create a chevron plot (Figure 6, inset). In other RNases H, we observed a rollover in the folding limb, which is attributed to the presence of a folding intermediate. In contrast, in the case of CtepRNH*, because of the dominating signal from the burst phase in low concentrations of urea, the observed rate was not fit at low denaturant concentrations, and therefore, there is no obvious rollover in the folding limb in this plot. On the other hand, we observed a distinct rollover in the CtepRNH* unfolding limb, suggesting the presence of an unfolding intermediate, that is not seen in other RNases H. Studies on other RNases H were limited in the range of denaturants accessible, but in this case, we were able to obtain data at denaturant concentrations much higher than the midpoint of the transition. Thus, it is not clear if this potential unfolding intermediate is a unique or general feature for this family of enzymes. Further investigation probing the possibility of an unfolding intermediate is underway. In sum, the kinetic refolding study on CtepRNH* shows that, much like

EcoRNH*, it folds through an apparent three-state pathway. By analogy to the other RNases H, it is likely that this intermediate is composed of the same core region known to be a dominant factor in encoding the unusually low ΔC_p of thermophilic RNase H.

DISCUSSION

Our previous studies on the stability profiles and folding pathways of two homologous RNases H (one from the mesophile *E. coli* and the other from the thermophile *T. thermophilus*) indicated that the ability of the TthRNH to function at high temperatures may depend on its unusually low change in heat capacity upon unfolding (ΔC_p) (*16*) and that the hydrophobic core of the thermophilic protein was the region responsible for the low ΔC_p. To probe the generality of these features, we identified and characterized a third homologous RNase H from the moderately thermophilic organism *C. tepidum*, with an optimal growth temperature between those of the two previously studied RNases H. All three proteins show pairwise sequence identities of $> 50\%$.

The three RNases H studied contain several free cysteines in their wild-type sequences [*E. coli* (three), *T. thermophilus* (four), and *C. tepidum* (three)]. Our previous studies on the energetics and folding of both *E. coli* RNase H and *T. thermophilus* RNase H were conducted on cysteine-free variants. Therefore, for ease of comparison, purification, and data collection, we created a similar variant for *C. tepidum* RNase H-CtepRNH*. Since the three free cysteines in CtepRNH are found in positions homologous to the positions of the three free cysteines in the *E. coli* protein, all three were mutated to alanine, as in EcoRNH*. As with the other two proteins, the cysteine-free variants are all active and maintain wild-type-like stability and melting temperatures. While it would be most informative to ascertain the activity of these RNases H at varying temperatures, because of the instability of the substrate at higher temperatures, the activity of each protein at the organism's growth temperature cannot be determined and compared.

The crystal structure of CtepRNH* revealed the typical RNaseH-like fold. The similarity of the α-carbon rmsds and the solvent-accessible surface areas (SASA) of RNases H from *E. coli*, *C. tepidum*, and *T. thermophilus* and TCEO (a chimera of *T. thermophilus* and *E. coli*) indicates that any differences among these three proteins are not the result of any major structural feature and depend on either more subtle structural differences or features of their energy landscapes (*1*, *19*, *23*). We did not directly compare the details of our structure to any additional RNase H structures, such as those from humans, *Sulfolobus tokodaii*, *Bacillus halodurans*, and some retroviruses, since these have notable structural differences, often lacking specific secondary structural elements such as the basic loop (*38*−*42*).

Analysis of the protein stability curve shows a ΔC_p for CtepRNH* that is much lower than both that of EcoRNH* and the value predicted on the basis of our crystal structure for CtepRNH*. Previous studies have experimentally determined that the change in heat capacity upon unfolding correlates with the change in hydrophobic solvent-accessible surface area upon unfolding (*22*, *43*). Calculating the expected change in SASA upon unfolding based on the crystal structure predicts a ΔC_p for CtepRNH* between 2.1 and 2.4 kcal mol^{-1} K^{-1}, while our stability curve shows the ΔC_p to be 1.7 kcal mol^{-1} K^{-1}. The ΔC_p determined by our data is quite close to that of TthRNH* (1.8 kcal mol^{-1} K^{-1}), while that of the mesophilic protein EcoRNH* (2.7 kcal mol^{-1} K^{-1}) is very close to the calculated value. On the basis of the crystal structures, it is predicted that these three homologous RNases H* should have quite similar ΔC_p values. The ΔC_p values from the stability curve data, however, differ by nearly 50%, leading to the hypothesis that both thermophilic RNases H* may have some residual structure in the unfolded state (*24*) and that a low ΔC_p may be a common feature of RNases H from even moderately thermophilic organisms.

Previous work has shown that the hydrophobic core of RNase H has a major role in determining the ΔC_p. A sequence alignment of all three RNases H shows that the core of CtepRNH* is more similar to the core of TthRNH* than to that of EcoRNH* (62% identical vs 54% identical). This similarity may indicate that the hydrophobic core of CtepRNH*, like that of TthRNH*, retains some structure in the unfolded state, resulting in a surprisingly low ΔC_p and perhaps playing a key role in determining the protein's thermophilic behavior.

While CtepRNH* shares some important similarities with TthRNH*, including a low ΔC_p and reversible heat denaturation, both its maximum stability and melting temperature are very close to those of EcoRNH*. It appears that CtepRNH* represents a case in which these thermodynamic features (melting temperature, change in heat capacity upon unfolding, or maximum stability) have evolved independently from one another. Despite the differences in thermodynamic parameters, the stabilities of all three proteins at the optimal growth temperatures of each organism are remarkably similar (5.6 kcal mol^{-1} for *T. thermophilus*, 6.8 kcal mol^{-1} for *E. coli*, and 4.6 kcal mol^{-1} for *C. tepidum*).

The folding pathway of CtepRNH* appears to share features with both previously studied RNases H*. This moderately thermophilic protein populates a stable, partially folded intermediate very early in the folding pathway. Analysis of the burst phase signal indicates that the stability of the intermediate of CtepRNH* is 4.1 kcal/mol, while the intermediates of EcoRNH* and TthRNH* have stabilities of 3.6 and 4.5 kcal/mol, respectively. Previous results suggest that the stability of the intermediate of CtepRNH* should result in an increased stability of the overall protein relative to EcoRNH*, as the stabilities of the intermediates of EcoRNH* and TthRNH* account for ∼35% of their overall stability. We have found that despite the increased stability of the intermediate, the overall stability of CtepRNH* is very close to that of EcoRNH*, meaning that the intermediate of CtepRNH* accounts for ∼50% of the global stability of the protein.

Because of the increased relative stability of the intermediate, we had concerns that the protein was populating the intermediate in our experiments, invalidating the two-state approximation used to fit our equilibrium denaturation and obtain the ΔG_{unf} values. However, this does not appear to be the case for several reasons. First, our denaturant data obtained via different methods are coincident, suggestive of a two-state transition. Second, a breakdown of the two-state assumption due to a notable population of an intermediate is known to result in an artificially low *m* value (*44*, *45*). Homologous proteins are expected to exhibit similar *m* values (*22*), and our calculated *m* value is within error of those obtained for other RNases H where the two-state assumption has been validated by modeling based on extensive kinetic data, including the transient intermediate (*45*). Finally, modeling of our system, including the small population of the intermediate, does not significantly alter the

stability profile we obtain. We believe, therefore, that the unusually low ΔC_p is not a direct consequence of the population of the intermediate. The low ΔC_p likely arises from residual structure in the unfolded state localized to this same core region, as demonstrated for TthRNH*.

The differences in the energetic properties of the RNases H underscore the subtlety of interactions leading to thermal stability. While it may be possible to increase the melting temperature of a protein through simple substitutional mutation, maintaining the finely tuned relationship among enzymatic activity, dynamics, and energetics that is required by biology at different temperature ranges clearly necessitates a more complex approach. Indeed, mutagenesis studies in which residues in *E. coli* RNase H were replaced with their counterparts from *T. thermophilus* RNase H have resulted in the classification of some residues as "thermophilic" due to the increased T_m of the protein upon substitution (*12*, *46*, *47*). These stabilizing mutations do not, however, recapitulate the thermodynamic profile we observe for thermophilic proteins. In fact, a recent structural thermodynamic study of one such quintuple mutant of *E. coli* RNase H reveals a maintained mesophile-like ΔC_p with an increase in T_m (*13*), indicating that while the mutant protein is more thermally stable, it is not actually recapitulating the "thermophilic behavior" characteristic of the other RNases H (Table 2). Interestingly, many of these so-called thermophilic residues are also found in *C. tepidum* RNase H, including an inserted Gly present in *T. thermophilus* and *C. tepidum* but not in *E. coli* RNase H (Figure 1) (*48*). However, *C. tepidum* RNase H behaves quite differently from the mutant *E. coli* RNase H, serving as a strong confirmation that simple residue substitution cannot fully govern thermal stability.

Our studies indicate that the RNase H family may employ an unusually low ΔC_p as a general strategy for achieving thermophilicity and that this likely represents a mechanism utilized by other protein families. Our results show that thermal stability (as defined by T_m) does not necessarily correlate with thermophilicity, as shown by the similarity in T_m values between CtepRNH* and EcoRNH*. The similarities in the folding pathway we observe among the different RNases H also suggest that all members of this family encode a marginally stable core of the protein that encompasses an early folding intermediate. The folding intermediate observed for RNase H from *C. tepidum* is likely composed of the same core region as seen by native state and pulsed labeling hydrogen exchange for both the *E. coli* and *T. thermophilus* RNases H. By analogy, we expect that the low ΔC_p of *C. tepidum* RNase H arises from residual structure in the unfolded state encoded by this same core region. On the basis of this work, it should be possible to design sequences of RNases H that display the desired thermophilic or mesophilic properties as defined by their ΔC_p and, therefore, fine-tune the energy landscape in a predictable fashion.

ACKNOWLEDGMENT

We thank Rachel Bernstein for critical reading of the manuscript and James Berger for crystallographic supplies and help.

REFERENCES

1. Ishikawa, K., Okumura, M., Katayanagi, K., Kimura, S., Kanaya, S., Nakamura, H., and Morikawa, K. (1993) Crystal structure of ribonuclease H from *Thermus thermophilus* HB8 refined at 2.8 Å resolution. *J. Mol. Biol.230*, 529–542.
2. Goedken, E. R., Keck, J. L., Berger, J. M., and Marqusee, S. (2000) Divalent metal cofactor binding in the kinetic folding trajectory of *Escherichia coli* ribonuclease HI. *Protein Sci.9*, 1914–1921.
3. Knapp, S., de Vos, W. M., Rice, D., and Ladenstein, R. (1997) Crystal structure of glutamate dehydrogenase from the hyperthermophilic eubacterium *Thermotoga maritima* at 3.0 Å resolution. *J. Mol. Biol.267*, 916–932.
4. Knapp, S., Kardinahl, S., Hellgren, N., Tibbelin, G., Schafer, G., and Ladenstein, R. (1999) Refined crystal structure of a superoxide dismutase from the hyperthermophilic archaeon *Sulfolobus acidocaldarius* at 2.2 Å resolution. *J. Mol. Biol.285*, 689–702.
5. Korndorfer, I., Steipe, B., Huber, R., Tomschy, A., and Jaenicke, R. (1995) The crystal structure of holo-glyceraldehyde-3-phosphate dehydrogenase from the hyperthermophilic bacterium *Thermotoga maritima* at 2.5 Å resolution. *J. Mol. Biol.246*, 511–521.
6. Szilagyi, A., and Zavodszky, P. (2000) Structural differences between mesophilic, moderately thermophilic and extremely thermophilic protein subunits: Results of a comprehensive survey. *Structure8*, 493–504.
7. Altschul, S. F., Gish, W., Miller, W., Myers, E. W., and Lipman, D. J. (1990) Basic local alignment search tool. *J. Mol. Biol.215*, 403–410.
8. Spassov, V. Z., Karshikoff, A. D., and Ladenstein, R. (1995) The optimization of protein-solvent interactions: Thermostability and the role of hydrophobic and electrostatic interactions. *Protein Sci.4*, 1516–1527.
9. Berezovsky, I. N., and Shakhnovich, E. I. (2005) Physics and evolution of thermophilic adaptation. *Proc. Natl. Acad. Sci. U.S.A.102*, 12742–12747.
10. Zeldovich, K. B., Berezovsky, I. N., and Shakhnovich, E. I. (2007) Protein and DNA sequence determinants of thermophilic adaptation. *PLoS Comput. Biol.3*, No. e5.
11. Tanner, J. J., Hecht, R. M., and Krause, K. L. (1996) Determinants of enzyme thermostability observed in the molecular structure of *Thermus aquaticus* D-glyceraldehyde-3-phosphate dehydrogenase at 25 Å Resolution. *Biochemistry35*, 2597–2609.
12. Kimura, S., Nakamura, H., Hashimoto, T., Oobatake, M., and Kanaya, S. (1992) Stabilization of *Escherichia coli* ribonuclease HI by strategic replacement of amino acid residues with those from the thermophilic counterpart. *J. Biol. Chem.267*, 21535–21542.
13. Haruki, M., Tanaka, M., Motegi, T., Tadokoro, T., Koga, Y., Takano, K., and Kanaya, S. (2007) Structural and thermodynamic analyses of *Escherichia coli* RNase HI variant with quintuple thermostabilizing mutations. *FEBS J.274*, 5815–5825.
14. Bae, E., and Phillips, G. N.Jr. (2004) Structures and analysis of highly homologous psychrophilic, mesophilic, and thermophilic adenylate kinases. *J. Biol. Chem.279*, 28202–28208.
15. Christodoulou, E., and Vorgias, C. E. (2002) The thermostability of DNA-binding protein HU from mesophilic, thermophilic, and extreme thermophilic bacteria. *Extremophiles6*, 21–31.
16. Hollien, J., and Marqusee, S. (1999) A thermodynamic comparison of mesophilic and thermophilic ribonucleases H. *Biochemistry38*, 3831–3836.
17. Topping, T. B., and Gloss, L. M. (2004) Stability and folding mechanism of mesophilic, thermophilic and hyperthermophilic archael histones: The importance of folding intermediates. *J. Mol. Biol.342*, 247–260.
18. Razvi, A., and Scholtz, J. M. (2006) Lessons in stability from thermophilic proteins. *Protein Sci.15*, 1569–1578.
19. Katayanagi, K., Miyagawa, M., Matsushima, M., Ishikawa, M., Kanaya, S., Nakamura, H., Ikehara, M., Matsuzaki, T., and Morikawa, K. (1992) Structural details of ribonuclease H from *Escherichia coli* as refined to an atomic resolution. *J. Mol. Biol.223*, 1029–1052.
20. Hollien, J., and Marqusee, S. (1999) Structural distribution of stability in a thermophilic enzyme. *Proc. Natl. Acad. Sci. U.S.A.96*, 13674–13678.
21. Chamberlain, A. K., Handel, T. M., and Marqusee, S. (1996) Detection of rare partially folded molecules in equilibrium with the native conformation of RNaseH. *Nat. Struct. Biol.3*, 782–787.
22. Myers, J. K., Pace, C. N., and Scholtz, J. M. (1995) Denaturant m values and heat capacity changes: Relation to changes in accessible surface areas of protein unfolding. *Protein Sci.4*, 2138–2148.
23. Robic, S., Berger, J. M., and Marqusee, S. (2002) Contributions of folding cores to the thermostabilities of two ribonucleases H. *Protein Sci.11*, 381–389.
24. Robic, S., Guzman-Casado, M., Sanchez-Ruiz, J. M., and Marqusee, S. (2003) Role of residual structure in the unfolded state of a thermophilic protein. *Proc. Natl. Acad. Sci. U.S.A.100*, 11345–11349.
25. Guzman-Casado, M., Parody-Morreale, A., Robic, S., Marqusee, S., and Sanchez-Ruiz, J. M. (2003) Energetic evidence for formation of a

pH-dependent hydrophobic cluster in the denatured state of *Thermus thermophilus* ribonuclease H. *J. Mol. Biol.329*, 731–743.
26. Eisen, J. A., Nelson, K. E., Paulsen, I. T., Heidelberg, J. F., Wu, M., Dodson, R. J., Deboy, R., Gwinn, M. L., Nelson, W. C., Haft, D. H., Hickey, E. K., Peterson, J. D., Durkin, A. S., Kolonay, J. L., Yang, F., Holt, I., Umayam, L. A., Mason, T., Brenner, M., Shea, T. P., Parksey, D., Nierman, W. C., Feldblyum, T. V., Hansen, C. L., Craven, M. B., Radune, D., Vamathevan, J., Khouri, H., White, O., Gruber, T. M., Ketchum, K. A., Venter, J. C., Tettelin, H., Bryant, D. A., and Fraser, C. M. (2002) The complete genome sequence of *Chlorobium tepidum* TLS, a photosynthetic, anaerobic, green-sulfur bacterium. *Proc. Natl. Acad. Sci. U.S.A.99*, 9509–9514.
27. Doering, D. S., and Matsudaira, P. (1996) Cysteine scanning mutagenesis at 40 of 76 positions in villin headpiece maps the F-actin binding site and structural features of the domain. *Biochemistry35*, 12677–12685.
28. Santoro, M. M., and Bolen, D. W. (1992) A test of the linear extrapolation of unfolding free energy changes over an extended denaturant concentration range. *Biochemistry31*, 4901–4907.
29. Becktel, W. J., and Schellman, J. A. (1987) Protein stability curves. *Biopolymers26*, 1859–1877.
30. Jones, T. A., Zou, J. Y., Cowan, S. W., and Kjeldgaard, M. (1991) Improved methods for building protein models in electron density maps and the location of errors in these models. *Acta Crystallogr.A47* (Part 2), 110–119.
31. Murshudov, G. N., Vagin, A. A., and Dodson, E. J. (1997) Refinement of macromolecular structures by the maximum-likelihood method. *Acta Crystallogr.D53*, 240–255.
32. Lee, B., and Richards, F. M. (1971) The interpretation of protein structures: Estimation of static accessibility. *J. Mol. Biol.55*, 379–400.
33. DeLano, W. L. (2002) The PyMOL Molecular Graphics System, DeLano Scientific, San Carlos, CA.
34. Kanaya, S., Kimura, S., Katsuda, C., and Ikehara, M. (1990) Role of cysteine residues in ribonuclease H from *Escherichia coli*. Site-directed mutagenesis and chemical modification. *Biochem. J.271*, 59–66.
35. Black, C. B., and Cowan, J. A. (1994) Magnesium activation of ribonuclease H: Evidence for one catalytic metal ion. *Inorg. Chem.33*, 5805–5808.
36. Pace, C. N., and Laurents, D. V. (1989) A new method for determining the heat capacity change for protein folding. *Biochemistry28*, 2520–2525.
37. Cecconi, C., Shank, E. A., Bustamante, C., and Marqusee, S. (2005) Direct observation of the three-state folding of a single protein molecule. *Science309*, 2057–2060.
38. You, D. J., Chon, H., Koga, Y., Takano, K., and Kanaya, S. (2007) Crystal structure of type 1 ribonuclease H from hyperthermophilic archaeon *Sulfolobus tokodaii*: Role of arginine 118 and C-terminal anchoring. *Biochemistry46*, 11494–11503.
39. Nowotny, M., Gaidamakov, S. A., Crouch, R. J., and Yang, W. (2005) Crystal structures of RNase H bound to an RNA/DNA hybrid: Substrate specificity and metal-dependent catalysis. *Cell121*, 1005–1016.
40. Davies, J. F.II, Hostomska, Z., Hostomsky, Z., Jordan, S. R., and Matthews, D. A. (1991) Crystal structure of the ribonuclease H domain of HIV-1 reverse transcriptase. *Science252*, 88–95.
41. Das, D., and Georgiadis, M. M. (2004) The crystal structure of the monomeric reverse transcriptase from Moloney murine leukemia virus. *Structure12*, 819–829.
42. Nowotny, M., Gaidamakov, S. A., Ghirlando, R., Cerritelli, S. M., Crouch, R. J., and Yang, W. (2007) Structure of human RNase H1 complexed with an RNA/DNA hybrid: Insight into HIV reverse transcription. *Mol. Cell28*, 264–276.
43. Gomez, J., Hilser, V. J., Xie, D., and Freire, E. (1995) The heat capacity of proteins. *Proteins22*, 404–412.
44. Mayne, L., and Englander, S. W. (2000) Two-state vs. multistate protein unfolding studied by optical melting and hydrogen exchange. *Protein Sci.9*, 1873–1877.
45. Spudich, G., and Marqusee, S. (2000) A change in the apparent m value reveals a populated intermediate under equilibrium conditions in *Escherichia coli* ribonuclease HI. *Biochemistry39*, 11677–11683.
46. Ishikawa, K., Kimura, S., Kanaya, S., Morikawa, K., and Nakamura, H. (1993) Structural study of mutants of *Escherichia coli* ribonuclease HI with enhanced thermostability. *Protein Eng.6*, 85–91.
47. Kimura, S., Kanaya, S., and Nakamura, H. (1992) Thermostabilization of *Escherichia coli* ribonuclease HI by replacing left-handed helical Lys95 with Gly or Asn. *J. Biol. Chem.267*, 22014–22017.
48. Ishikawa, K., Nakamura, H., Morikawa, K., Kimura, S., and Kanaya, S. (1993) Cooperative stabilization of *Escherichia coli* ribonuclease HI by insertion of Gly-80b and Gly-77 → Ala substitution. *Biochemistry32*, 7136–7142.